Effects of Mobile Buffers on Facilitation: Experimental and Computational Studies

Yun-gui Tang, Thomas Schlumpberger, Tae-sung Kim, Martin Lueker, and Robert S. Zucker
Molecular and Cell Biology Department, Neurobiology Division, University of California, Berkeley, California 94720 USA

ABSTRACT Facilitation is an important form of short-term plasticity that occurs in most synapses. At crayfish neuromuscular junctions, basal transmission and facilitation were significantly reduced after presynaptic introduction of "fast" high-affinity calcium buffers, and the decay of facilitation was accelerated. The existence of residual calcium during facilitation was also demonstrated. Computational modeling of three-dimensional buffered Ca^{2+} diffusion and binding to secretory and facilitation targets suggest that the facilitation site is located away from a secretory trigger mediating exocytosis; otherwise, the facilitation site would be saturated by each action potential. Our simulations account for many characteristics of facilitation and effects of exogenous buffer, and suggest that facilitation is caused by residual calcium gaining access to a site distinct from the secretory trigger through restricted diffusion.

INTRODUCTION

In facilitation, a second action potential causes more transmitter release than the first. Calcium entry is necessary for facilitation (Katz and Miledi, 1968), but how calcium causes facilitation is unclear. Presynaptic calcium accumulating during repetitive activity, often termed "residual calcium," may cause facilitation (reviewed in Zucker, 1994, 1999).

In support of the "residual calcium" hypothesis, facilitation is virtually abolished if accumulated presynaptic calcium is reduced by photolysis of diazo-2, a BAPTA-like Ca^{2+} chelator (Kamiya and Zucker, 1994; Fischer et al., 1997). Mobile exogenous buffers should reduce accumulation of residual calcium and speed its diffusion away from the active zone, reducing facilitation and accelerating its decay if residual calcium is responsible for facilitation. Numerous studies (e.g., Atluri and Regehr, 1996; others reviewed in Zucker, 1994, 1999), including some at crayfish neuromuscular junctions (Delaney et al., 1991; Hochner et al., 1991) report such results. However, other researchers (e.g., Tanabe and Kijima, 1989), some also working with crayfish junctions (Winslow et al., 1994), report that facilitation is not affected by such buffers. These authors, and others suggesting that residual calcium decays much faster than facilitation (Blundon et al., 1993), propose that calcium entering during an action potential activates facilitation despite the return of residual calcium to resting levels. Simulations based on the assumption that facilitation is due to the action of bound calcium that entered during the action potential have also appeared (Yamada and Zucker, 1992; Bertram et al., 1996). It must be stressed that such a model remains inconsistent with the experimental findings of Kamiya and Zucker (1994), Atluri and Regehr (1996), and Fischer et al. (1997), among others.

A second issue is whether calcium necessarily acts at a site distinct from the secretory trigger to generate facilitation. At many synapses residual calcium is in the micromolar or submicromolar range following repetitive activity (reviewed in Zucker, 1994, 1999). It is therefore impossible that facilitation occurs through simple summation of residual calcium with the $\sim$50 μM local calcium elevation during an action potential needed to evoke phasic transmitter release (Adler et al., 1991; Llinás et al., 1992; Heidelberger et al., 1994; Landò and Zucker, 1994), despite the highly nonlinear relationship between $[Ca^{2+}]_i$ and transmitter release. Calcium therefore acts in facilitation at a high-affinity target distinct from the low-affinity site triggering exocytosis.

In order to understand facilitation we need to know the spatiotemporal dynamics of $[Ca^{2+}]_i$ in nerve terminals. However, exocytosis occurs in the immediate vicinity of calcium channels, where the relevant local $[Ca^{2+}]_i$ cannot be measured directly due to the limited spatiotemporal resolution of current $[Ca^{2+}]_i$ detection methodologies. Computational simulation of calcium kinetics and facilitation models provides a useful alternative (Yamada and Zucker, 1992; Winslow et al., 1994; Cooper et al., 1996). We have used such modeling to investigate whether a set of binding kinetics, affinity, and location of secretory trigger and facilitation site can be found that account for the characteristics of facilitation and effects of exogenous calcium buffers.

MATERIALS AND METHODS

We used first walking legs of 2–2.5-inch crayfish (*Procambarus clarkii*) from Atchafalaya Biological Supplies (Raceland, LA) or Niles (Sacramento, CA). Opener muscles and motor nerves were exposed in normal Van Harreveld's solution containing (in mM) 195 NaCl, 13.5 $CaCl_2$, 5.4

Received for publication 4 November 1999 and in final form 21 February 2000.

Address reprint requests to Robert S. Zucker, Molecular and Cell Biology Department, Neurobiology Division, 111 Life Sciences Addition, University of California, Berkeley, CA 94720-3200. Tel.: 510-642-3407; Fax: 510-643-6791; E-mail: zucker@socrates.berkeley.edu.

Y-g. Tang and T. Schlumpberger contributed equally to this work.

0006-3495/00/06/2735/17 $2.00

KCl, 2.6 $MgCl_2$, and 10 Na-HEPES at pH 7.4. Excitor or inhibitor axons were stimulated with suction electrodes on nerve bundles in the meropodite. Temperature was 16–19°C, but varied <0.5°C in any experiment.

Electrophysiology

Excitatory junctional potentials (EJPs) or inhibitory junctional potentials (IJPs) were recorded from the most proximal muscle fibers, and digitized using pClamp 6.0 (Axon Instruments, Foster City, CA). Stable IJPs were recorded with 3–6 MΩ microelectrodes filled with 3 M KCl at least 1 h after the cell was penetrated to allow stabilization of the chloride equilibrium potential. To further assure stability of IJP amplitudes, an average of ten 10-pulse 100-Hz trains separated by 10-s intervals was collected every 20 min, before accepting a preparation for study of inhibitory transmission. The value of the chloride equilibrium potential was assessed by measuring inhibitory junctional currents at different potentials using a single-electrode voltage clamp (Dagan 8000, Dagan Corp., Minneapolis, MN).

To minimize the distortion of results by noise and fluctuations in transmitter release, we averaged 30–60 JPs and optical signals (see below). To minimize accumulation of short-term plasticity, successive 5-pulse trains were separated by at least 5 s, and 15-pulse trains by at least 15 s, resulting in an average stimulation frequency of ≤1 Hz.

EJP amplitudes during a tetanus were obtained by subtracting peak amplitude from the extrapolated falling phase of the previous EJP and correcting for the nonlinear relationship between postsynaptic potential and transmission (Martin, 1955), assuming an EJP reversal potential of +23 mV (Onodera and Takeuchi, 1978). Martin correction of IJP amplitudes used chloride equilibrium potential measurements from each experiment. Curve fitting was performed with Prism (GraphPad Software, San Diego, CA) using a least-squares algorithm to estimate time constants of facilitation. All results are presented as mean ± SD. Statistical significance was assessed with two-sided paired Student's *t*-tests.

Exogenous buffer was introduced into nerve terminals by including BAPTA-AM in the bath or by injecting fura-2 into the axon. In the former case, EJPs were recorded at least 1 h after the solution was changed to 1% vol/vol dimethyl sulfoxide (DMSO) in Van Harreveld's solution as control, and then recorded 1 h after changing to a solution with 50 μM BAPTA-AM and 1% DMSO. This solution was made by 100:1 dilution of a stock solution of 5 mM BAPTA-AM in DMSO into Van Harreveld's solution, stored at −20°C. Fura-2 (K-salt) was dissolved at 17 mM in 200 mM KCl and iontophoresed into the Y branch of the motor axon using 10–15 nA of hyperpolarizing current for 5–10 min, until fura-2 concentration in boutons reached 400 μM estimated fluorometrically (Delaney et al., 1989). Control responses were recorded after the axon was penetrated, but before iontophoresis.

Intraterminal calcium measurement

$[Ca^{2+}]_i$ in nerve terminals was measured using fura-2 fluorescence detected with a photomultiplier tube (PMT, Hamamatsu Corp., San Jose, CA) through a long-working-distance 40× Olympus (Lake Success, NY) water immersion objective. A xenon lamp excited fluorescence through filters of 360 ± 10 nm and 382 ± 5 nm (Omega Optics, Brattleboro, VT). A dichroic mirror (455 nm, Nikon, Japan) separated excitation and emission lights, and a barrier filter (530 ± 20 nm, Omega Optics) limited interference from autofluorescence.

Fluorescence was restricted to single boutons by use of a field diaphragm interposed in front of the PMT. An average of 30–50 recordings at 15-s intervals of 382-nm excited fluorescence intensity was acquired while the axon was stimulated for a brief period in the middle of the fluorescence recording, followed by a series of measurements of 360-nm excited fluorescence. An area near the bouton was used to measure the background fluorescence for 382 nm and 360 nm excitation. Averaged background fluorescence was subtracted from corresponding signals measured from the bouton. Because stimulation had no effect on fluorescence excited by 360 nm, the overall average over time of this fluorescence was used as a constant to divide the fluorescence signal excited by 382 nm to generate time-dependent fluorescence ratios. The bouton was only exposed to UV during acquisition of fluorescence data. Tetani of 15 pulses started 80 ms after the beginning of fluorescence measurements, while tetani of 5 pulses began 1 s after fluorescence measurement started.

Fura-2 (50 μM) was calibrated in vitro by measuring the fluorescence ratio in solutions resembling crayfish cytoplasm: 250 mM potassium gluconate, 15 mM NaCl, 15 mM K-HEPES, pH 7.02, with zero-calcium (10 mM K_2EGTA), 5 mM Ca^{2+}, or Ca^{2+} buffered to 500 nM with 10 mM K_2EGTA and 5 mM $CaCl_2$. The K_d of fura-2 for calcium was estimated as 360 nM. Ratios calculated in terminals were converted to $[Ca^{2+}]_i$ (Grynkiewicz et al., 1985) after application of a viscosity correction corresponding to a 30% reduction in minimum and maximum 382/360 nm fluorescence ratios (Delaney et al., 1989).

Implementing differential equations

To solve the differential equations of stage 1 modeling we used a numerical approach that transformed the differential equations into finite difference equations, where the nerve terminal was divided into spatial compartments and the time continuum was discretized into finite time steps. Transient calcium gradients are sharpest near the cell membrane in the vicinity of calcium channels. To reduce computation time, we doubled the linear compartment size at the 5th sheet of compartments away from the membrane, and doubled it again at the 9th and 14th sheets. Hence, compartments at the rear surface have a volume 512 times those at the synaptic surface.

Diffusion was computed using the explicit method of the finite-difference solution (Crank, 1975); representative for all species we show the calculation for the change in calcium concentration (ΔC) within one time step (Δt):

$$\Delta C = D\Delta t/\Delta x^2(C[x+1][y][z] + C[x-1][y][z] - 2C[x][y][z] + C[x][y+1][z] + C[x][y-1][z] - 2C[x][y][z] + C[x][y][z+1] + C[x][y][z-1] - 2C[x][y][z]).$$

Δx denotes the spatial resolution of a cubical compartment, so $\Delta x = \Delta y = \Delta z$. $C[x][y][z]$ denotes calcium concentration of a compartment at location x, y, and z, $C[x+1][y][z]$ the top neighbor to that compartment, etc. The time step Δt was significantly smaller than the limit imposed for stability of numerical solutions to the diffusion equation (Crank, 1975), because of even more severe restrictions imposed by fast buffer reactions. For Δx = 20 nm, Δt was 62.5 ns, while for Δx = 10 nm, Δt was 10 ns.

Each calcium buffer reaction was calculated using the first-order Euler scheme; representative for all species (calcium and up to two mobile buffers and one immobile species), we show the calculation for the change in calcium concentration ΔC based on the reaction of calcium with buffer B within one time step Δt:

$$\Delta C = \Delta t(k_{off}CB[x][y][z] - k_{on}C[x][y][z]B[x][y][z]).$$

Calcium extrusion was calculated using the finite difference approximation of a linear first-order differential equation of a surface pump:

$$\Delta C = P\Delta t/\Delta x(C[x][y][z] - C_0),$$

where C_0 denotes resting calcium and P denotes the pump rate. This equation represents a boundary condition at the rear and front surface of the terminal. The boundary condition of the remaining "walls" surrounding one active zone was zero flux. Calcium influx was implemented as a point source representing current through a single calcium channel streaming

into a compartment volume:

$$\Delta C = \Delta t/\Delta x^3(C_{\text{influx}}).$$

The first-order differential equations derived from the release schemes of stage 2 were solved numerically using finite-difference approximations (first-order Euler schemes). The system of differential equations yield a system of tridiagonal linear equations; this system was solved by using the tridiagonal algorithm (Press et al., 1988). All calculations were coded in C; intensive computations were run on Cray T2D and T90 supercomputers.

Monte Carlo simulations

Random walks were carried out in a simulation space of 250 × 250 × 80 nm divided into cubic cells 1 nm on a side. One surface of the cube represented the plasma membrane, on the center of which sat a 50-nm diameter vesicle perched on a docking complex represented by a 24-nm diameter cylinder 4 nm high. Docked vesicles appear to be lined up in a ring surrounding the calcium channels in an active zone (Cooper et al., 1996), so the width of the simulation space was set to 80 nm to represent the typical vesicle spacing. Each walk started from a calcium channel mouth located in the cell membrane 20 nm away from the center of the docking complex. At each time step, the walk proceeded randomly to one of the six adjacent cells along one of the three coordinate axes ($+x$ or $-x$, $+y$ or $-y$, $+z$ or $-z$). A random number generator with a 48-bit seed was used to ensure randomness. The plasma membrane, vesicle, and docking complex were impermeable; any step that would cross such a boundary resulted in no movement. The top surface 250 nm above the plasma membrane and the front and rear surfaces located 125 nm from the vesicle were simulation boundaries; crossing this boundary terminated a walk, representing that an ion that has diffused this far would almost never reach its target. The plasma membrane was impermeable, and so were the side surfaces between adjacent vesicles, reflecting symmetry of the calcium profiles due to adjacent vesicles and associated calcium channels. If a walk hit a target cell, the walk was terminated and the time taken (number of steps in the walk) to reach the target recorded. Histograms of these times are plotted for at least 3×10^5 walks.

In control simulation, diffusion into semi-infinite space was represented as into a 250-nm cubic region with only the bottom surface impermeable, and the target located 100 nm below or lateral to the calcium channel in the center of the membrane surface. To assure that the simulation space was large enough, a few simulations were run with a 500-nm cube, and the results were virtually identical. Likewise, simulations with 0.5-nm cells demonstrated that the cell size was sufficiently small. The Monte Carlo approximation to diffusion was validated by comparing histograms of diffusion times in simulations of unrestricted diffusion to the analytical solution of the diffusion equation for an instantaneous point source into semi-infinite space, measured at 100 nm below the source (Crank, 1975). The number of steps taken was converted to time using $T = l^2/6D_{\text{app}}$ to calculate a single step duration (T), where $l = 1$ nm and $D_{\text{app}} = (D_{\text{calcium}} + D_m \cdot \kappa_m)/(1 + \kappa_s + \kappa_m) = 10.8\ \mu\text{m}^2\ \text{s}^{-1}$ (see Gabso et al., 1997). Histogram amplitudes were converted to concentration C using $C = F \cdot P/(\kappa_e \cdot l^3)$, where F is the flux through a single calcium channel during an action potential (2.27×10^{-21} mol), and P is the proportion of walks resulting in hits on the target cell.

RESULTS

Reduction of transmission and facilitation by exogenous "fast" buffer

Accumulation of facilitation was measured using 5-pulse 100-Hz trains of excitatory motor neuron stimuli. The amplitude of the first EJP reflects basal transmission, and facilitation was calculated from $F_n = \text{EJP}_n/\text{EJP}_1 - 1$, where F_n = facilitation of the nth EJP.

Presynaptic buffer capacity was increased by introduction of exogenous calcium buffer. Transmission was reduced by 70.3 ± 7.0% (mean ± SD, $n = 5$, $p < 0.01$) 90 min after BAPTA-AM application, and by 66.6 ± 15.1% ($n = 5$, $p < 0.02$) after iontophoresis of 400 μM fura-2 into the nerve terminals (Figs. 1*A* and 2*A*), similar to results reported previously (Hochner et al., 1991; Winslow et al., 1994).

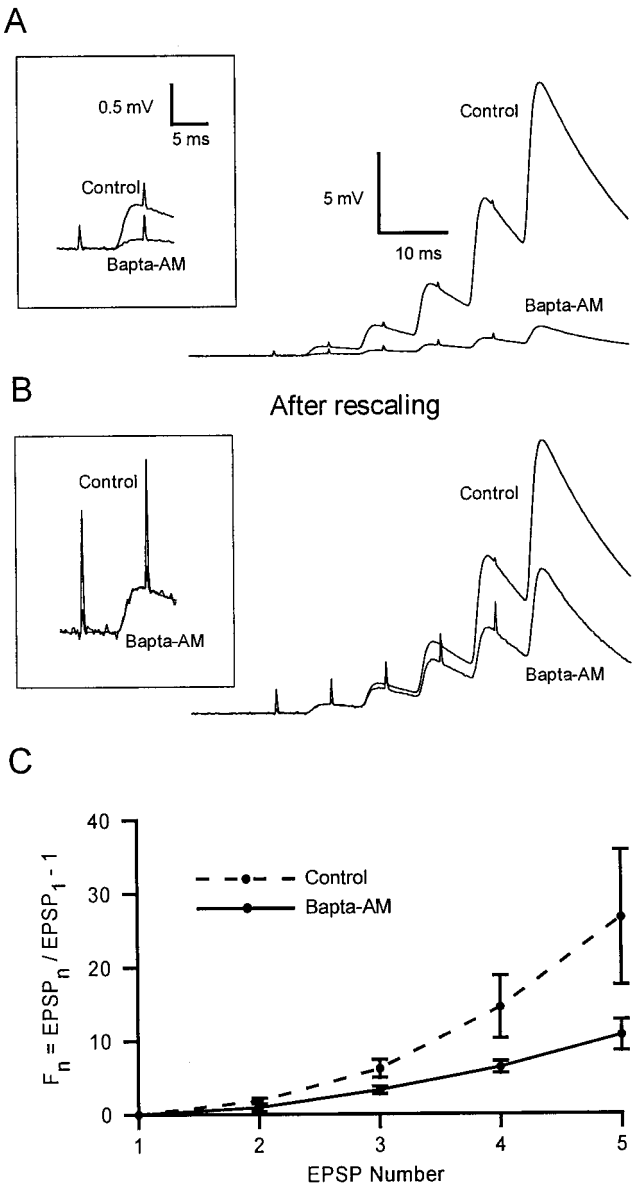

FIGURE 1 Effects of BAPTA-AM on transmission and facilitation. (*A*) Averaged responses of 5 EJPs at 100 Hz in the absence and presence of BAPTA-AM. Reduction in the first EJP is shown in the inset. (*B*) After rescaling to match initial EJP amplitudes (*inset*), a reduction in facilitation in BAPTA-AM is evident. (*C*) Summary of BAPTA-AM experiments, showing reduction in facilitation by BAPTA-AM.

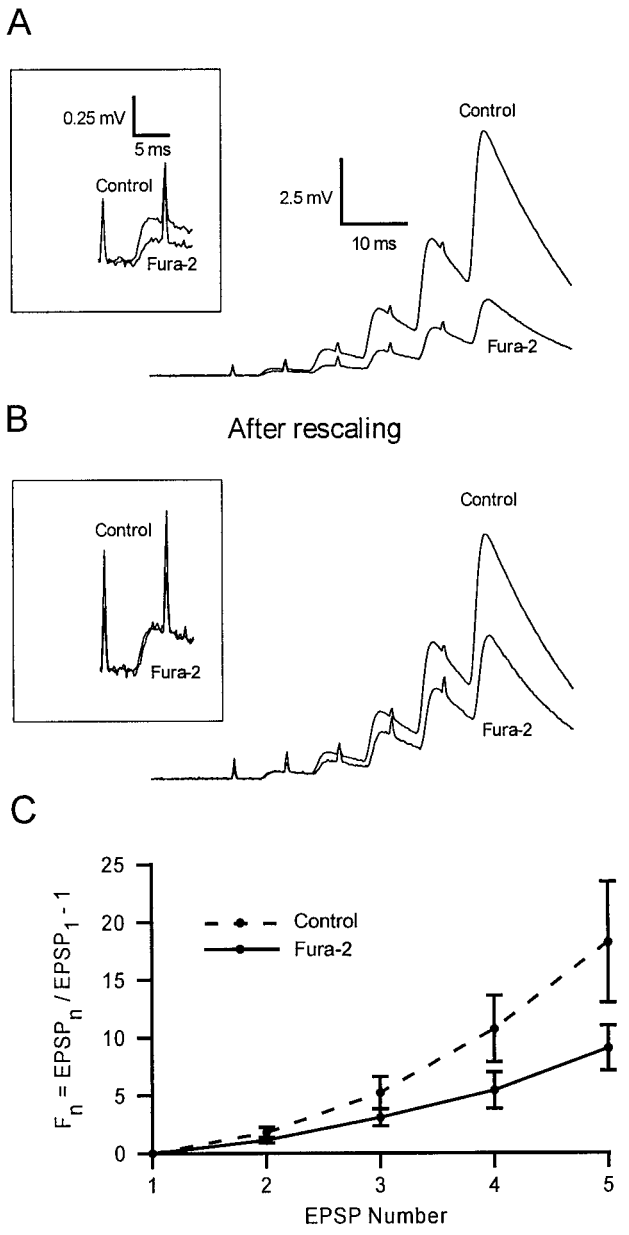

FIGURE 2 Effects of fura-2 on transmission and facilitation. Panels are arranged as in Fig. 1, except the exogenous buffer is 400 μM fura-2, which reduced both transmission and facilitation.

Exogenous buffers also reduced facilitation (Figs. 1 and 2). Rescaling records to match initial EJP amplitudes before and after addition of exogenous buffer shows that BAPTA-AM and fura-2 reduced facilitation of all subsequent EJPs. Reduction of facilitation from the second to the fifth stimulation is statistically significant in both treatments ($n = 5$ for each, $p < 0.05$).

The reduced accumulation of facilitation can be explained either by a reduction in the incremental facilitation added by each action potential and/or an accelerated decay of facilitation. To distinguish these possibilities, decay of facilitation was examined before and after fura-2 injection. A 4-pulse tetanus (100 Hz) was used as the conditioning stimulation, and facilitation of a test pulse delivered subsequently at different intervals (t) was plotted versus the interval. Fig. 3 shows the effects of fura-2 on the decay of facilitation. Facilitation is well-described as a sum of two exponential processes (Zucker, 1974):

$$F(t) = \text{Plateau} + F_1 \cdot \exp(-t/\tau_1) + F_2 \cdot \exp(-t/\tau_2)$$

where F_1 is the fast phase of facilitation immediately after the fourth pulse, F_2 is the slow component of facilitation, and τ_1 and τ_2 are the decay time constants of F_1 and F_2, respectively. The remaining small plateau probably represents a form of plasticity bearing a longer time course, such as augmentation (Delaney and Tank, 1994). The effects of exogenous buffers on all facilitation parameters from five experiments are summarized in Table 1. Both phases of facilitation are shortened by fura-2, and the fast phase especially is also reduced in magnitude. As shown below, these results are generally consistent with a residual calcium hypothesis of facilitation.

Residual calcium during facilitation

Previous simulations (Winslow et al., 1994) suggested that there would be virtually no residual calcium during facilitation in this preparation. Residual calcium has been measured during augmentation and post-tetanic potentiation (Delaney et al., 1989; Mulkey and Zucker, 1992; Delaney and Tank, 1994; Tang and Zucker, 1997) in crayfish, but until now not during facilitation.

A ratiometric measurement of calcium requires a stationary preparation. We have tried to block muscle movements with agents causing muscle detubulation, with L-type calcium channel blockers and with a variety of glutamate receptor antagonists, but have never been completely successful. Thus inhibitory nerve terminals were chosen to measure residual calcium. Fig. 4 *A* shows that a 5-pulse 100-Hz tetanus causes an ~50-nM calcium increase in inhibitory terminals. Similar experiments carried out on two other preparations showed a 15- and 22-nM calcium increase, respectively. The calcium increase during facilitation was more obvious when a longer tetanus was used to elicit facilitation. In six other experiments a 15-pulse 100-Hz tetanus increased calcium by 70–320 nM. Thus the residual calcium concentration increase induced by a single pulse is 9 ± 6 nM ($n = 9$). This result shows that residual calcium accumulates during stimulation that elicits facilitation with little augmentation or potentiation.

Because calcium measurements were done on inhibitory terminals, we checked that their facilitation is similar to that of excitatory synapses. IJPs were reversed and enlarged by loading muscle fibers with KCl to elevate the Cl-dependent IJP reversal potential, which stabilized to a level between

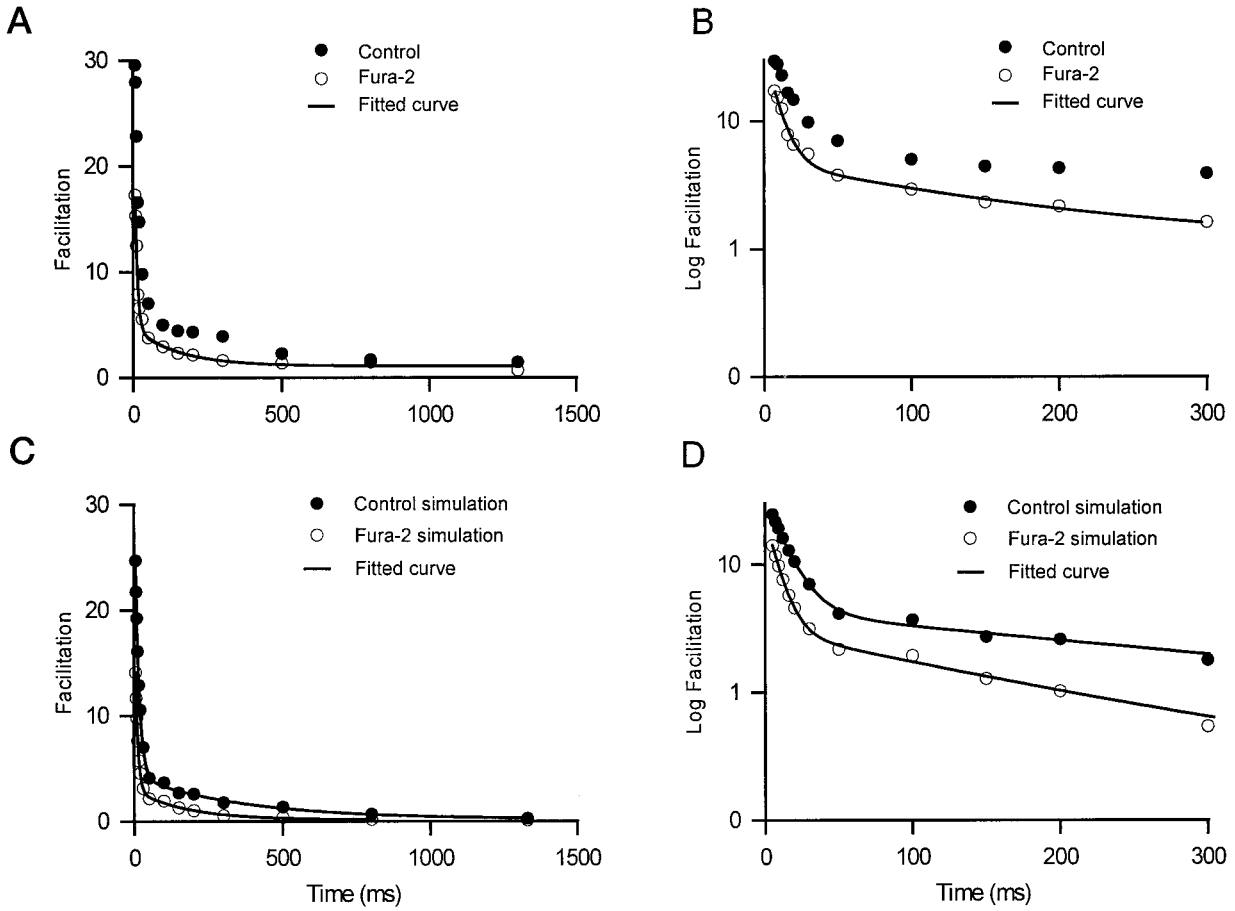

FIGURE 3 Fura-2 reduces facilitation and speeds its decay. (*A*) Example of decay of facilitation in the absence and presence of fura-2 in nerve terminals. Solid lines were fitted curves. The effects of fura-2 on the first component of facilitation is more clearly seen in (*B*) using semilogarithmic axes. (*C*) Time course of decay of facilitation in the absence (control) and the presence (fura-2) of fura-2 calculated with the X3Y1 spatial segregation model of three calcium ions binding to the secretory trigger (X) and 1 ion binding to the facilitation site (Y). Solid lines were fitted using a two-phase exponential decay; expansion of early points and lines shown in using semilogarithmic coordinates in (*D*).

−50 and −44 mV in four experiments and changed <5% over 3 h, as confirmed by voltage clamp measurements from resting potentials of −70 mV. IJP facilitation and effects of fura-2 injection were measured in six of these experiments, one of which is illustrated in Fig. 4, *B* and *C*.

IJPs are slower than EJPs, so that the rising phase of a following IJP starts before the previous IJP has reached its peak. This makes it difficult to distinguish individual IJP amplitudes in a train. In order to rescale responses before and after fura-2 injection, single IJPs were averaged and the ratio of their amplitudes was used to rescale the responses to trains so that the (indistinct) initial IJPs would be matched. Fura-2 reduced transmission assessed with single IJPs by 44.2 ± 13.4% ($n = 6$, $p < 0.01$), similar to the effect on EJPs. Because individual IJPs in a train were not discernible, cumulative facilitation was assessed from the peak of the summated IJPs after Martin (1955) correction using the measured IJP reversal potential. By this measure, fura-2 reduced facilitation by 23.3 ± 11.0% ($n = 6$, $p < 0.05$). Alternatively, in three relatively low-noise experiments we

TABLE 1 Effects of fura-2 on the decay of facilitation

	Initial EJP (mV)	F_1	τ_1 (ms)	F_2	τ_2 (ms)	Plateau
Control	0.33 ± 0.11	21.8 ± 12.5	18.6 ± 4.9	4.1 ± 1.2	536 ± 222	0.53 ± 0.51
Fura-2	0.14 ± 0.04	16.1 ± 8.9	12.2 ± 3.3	2.4 ± 1.0	365 ± 222	0.04 ± 0.64
t-value	4.852	3.237	4.054	2.610	3.577	3.306
P	<0.01	<0.05	<0.02	>0.05	<0.05	<0.05

Numbers are mean ± SD, $n = 5$.

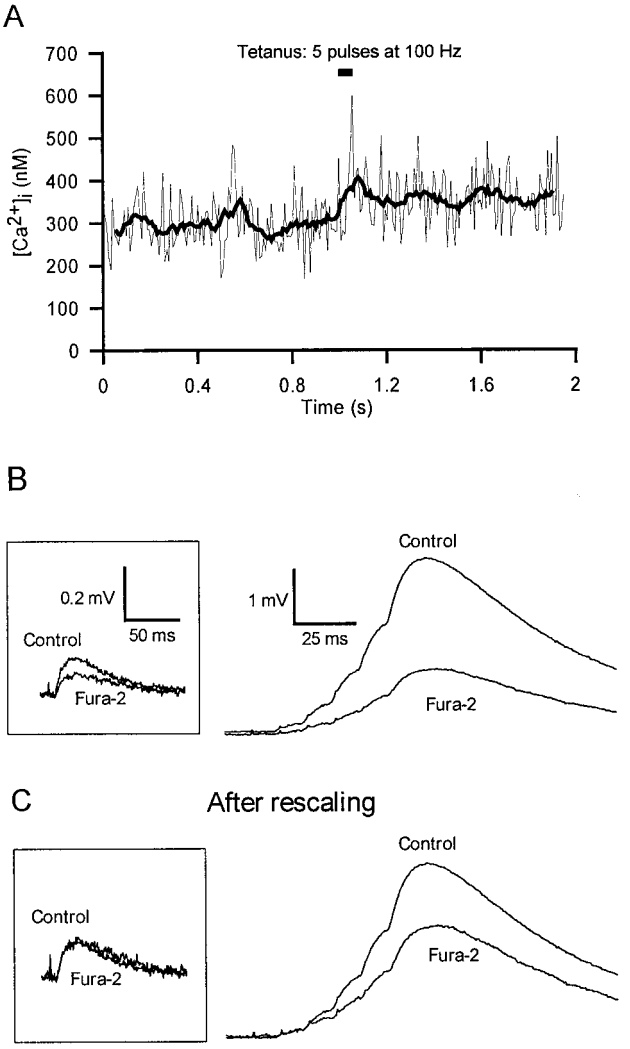

FIGURE 4 Residual calcium during facilitation and effects of fura-2 on transmission and facilitation of IJPs. (*A*) A 5-pulse 100-Hz train produces ~50 nM residual calcium. The heavy line in the middle is the running average of 13 points. (*B*) Fura-2 reduces IJP amplitudes. The insets show single IJPs before and after fura-2 injection. (*C*) After rescaling to match initial IJP amplitudes, showing reduction in facilitation.

compared the maximum slope of the fifth IJP before and after injection. The reduction was 37.4 ± 11.9% after fura-2 injection. Thus effects of presynaptic fura-2 injection on facilitation and transmission at inhibitory and excitatory synapses are similar, and the more precise measurements of effects on EJPs may be compared to the measurement of residual calcium at inhibitory synapses.

A two-stage presynaptic calcium diffusion-reaction model for facilitation

During action potentials, calcium enters nerve terminals through calcium channels, diffuses into the cytoplasm, and binds to calcium buffers. Calcium is removed from terminals by plasma membrane calcium pumps. The task of our model is to simulate these processes, and calculate the release of neurotransmitter and facilitation based on them.

Diffusion of concentration C of a substance is described by the second-order linear partial differential equation:

$$\frac{\partial C}{\partial t} = D\nabla^2 C.$$

Calcium buffering occurs according to the following reaction scheme, and the differential equation describes the change in calcium concentration due to the action of buffer B:

$$C + B \underset{k_{off}}{\overset{k_{on}}{\rightleftharpoons}} CB,$$

$$\left(\frac{\partial C}{\partial t}\right)_{buffer} = k_{off}[CB] - k_{on}[C][B].$$

The finite concentration of total buffer (B_{tot}) imposes limits on this reaction and the linear differential equation becomes nonlinear. If the endogenous buffer is even partly mobile, diffusion of this buffer influences calcium diffusion. Exploring effects of alien mobile buffers requires that their diffusion and reaction also be considered. Calcium influx and extrusion set specific boundary conditions. These constraints lead to a coupled system of equations describing how these species interact and shape the spatiotemporal patterns of intracellular calcium concentration ($[Ca^{2+}]_i$), denoted here by C, where amB represents alien mobile buffer, emB is the endogenous mobile buffer, and efB is the endogenous immobile buffer:

$$\frac{\partial \mathrm{amB}}{\partial t} = D\nabla^2 \mathrm{amB} + \left(\frac{\partial \mathrm{amB}}{\partial t}\right)_{calcium},$$

$$\left(\frac{\partial \mathrm{amB}}{\partial t}\right)_{calcium} = k_{off}[C\mathrm{amB}] - k_{on}[C][\mathrm{amB}],$$

$$\left(\frac{\partial \mathrm{efB}}{\partial t}\right)_{calcium} = k_{off}[C\mathrm{efB}] - k_{on}[C][\mathrm{efB}],$$

$$\frac{\partial \mathrm{emB}}{\partial t} = D\nabla^2 \mathrm{emB} + \left(\frac{\partial \mathrm{emB}}{\partial t}\right)_{calcium},$$

$$\left(\frac{\partial \mathrm{emB}}{\partial t}\right)_{calcium} = k_{off}[C\mathrm{emB}] - k_{on}[C][\mathrm{emB}],$$

$$\frac{\partial C}{\partial t} = D\nabla^2 C + \left(\frac{\partial C}{\partial t}\right)_{amB} + \left(\frac{\partial C}{\partial t}\right)_{emB} + \left(\frac{\partial C}{\partial t}\right)_{efB} + \left(\frac{\partial C}{\partial t}\right)_{|calcium} + \left(\frac{\partial C}{\partial t}\right)_{pump}.$$

Note that k_{off} and k_{on} are different for each buffer species. The total amount of any buffer species [B_{tot}] includes cal-

cium-free [B] and calcium-bound [CB] forms; [B_{tot}] = [B] + [CB] is spatially uniform if the buffer's diffusional mobility is unaffected by binding to calcium (Roberts, 1994).

Because calculation of spatiotemporal $[Ca^{2+}]_i$ profiles is computationally much heavier than calculation of the reaction schemes leading to transmitter release and facilitation, we break the problem into two stages: 1) calcium diffusion and buffering, and 2) calcium-receptor and subsequent reactions. This separation facilitates the exploration of different reaction schemes after determining a spatiotemporal $[Ca^{2+}]_i$ profile. The separation is legitimate because the binding of calcium to its targets in triggering secretion and facilitation involves so few calcium ions that local $[Ca^{2+}]_i$ is unaffected (Yamada and Zucker, 1992).

Stage 1 diffusion parameters

Crayfish presynaptic motor boutons are roughly spherical, with synaptic contacts located on one hemisphere facing the muscle. For simplicity we represent boutons as rectangular solids, and a hemispherical surface as three adjacent flat surfaces. Simplifying further, we place active zones on one surface of the bouton. One effect of this is to reduce the ratio of synapse density to bouton volume by a factor of three. To correct for this, we could triple the number of synapses located on the surface, but this would distort the overlap of calcium domains from neighboring synapses. Instead, to avoid near-membrane distortions, we reduce the volume of the bouton to one-third to match the reduction in overall synaptic surface area. The average bouton diameter in our preparations is 3 μm, which we represent with a rectangular solid whose volume is reduced to one-third by decreasing the distance from the synaptic face to the opposite surface of the bouton to 1 μm.

It is assumed that the kinetics of transmitter release are uniform at all synaptic contacts (active zones), so the time course of secretion and facilitation from one active zone is taken as representative of the whole synapse. The active zone exhibits two kinds of symmetry: 1) all except the most peripherally located synapses are surrounded by identically behaving synapses, and 2) each square active zone displays a fourfold symmetry. Thus, simulating a quarter of an active zone and its surrounding area (no calcium passes lateral boundaries due to symmetry) provides a simplified representation of an entire nerve terminal.

Cooper et al. (1996) describe the typical active zone as having a diameter of ~160 nm, containing 13–20 calcium channels, and surrounded by vesicles. Based on these findings, our active zone is a square with an edge of 160 nm in simulations using a 20-nm compartment size or spatial resolution (see Experimental Procedures). The active zone lies in the center of a 2.56 μm^2 space, which is in the middle of the observed range (Cooper et al., 1995). We place four calcium channels in each quarter active zone spaced 40 nm apart, with 60 nm separating channels from those of the adjacent quarter active zone (details in Schlumpberger, 1999). In simulations with 10-nm resolution, the active zone is square, 120 nm on a side, and the interchannel spacing is 30 nm. Vesicles are assumed to be docked just outside the outermost calcium channels, with the calcium-binding secretory target 10–20 nm below the nearest channel mouth. Fig. 5 illustrates some of these geometrical relationships.

Most calcium enters as a tail current following an action potential (Llinás et al., 1981). We represent the calcium influx (C_{influx}) as a 1-ms flux of 1.35×10^{-9} fM μs^{-1}, followed by a 0.2 ms tail current flux of 4.6×10^{-9} fM μs^{-1} (Yamada and Zucker, 1992).

We assumed the presence of mobile and immobile calcium buffers, based on recent measurements of Aplysia

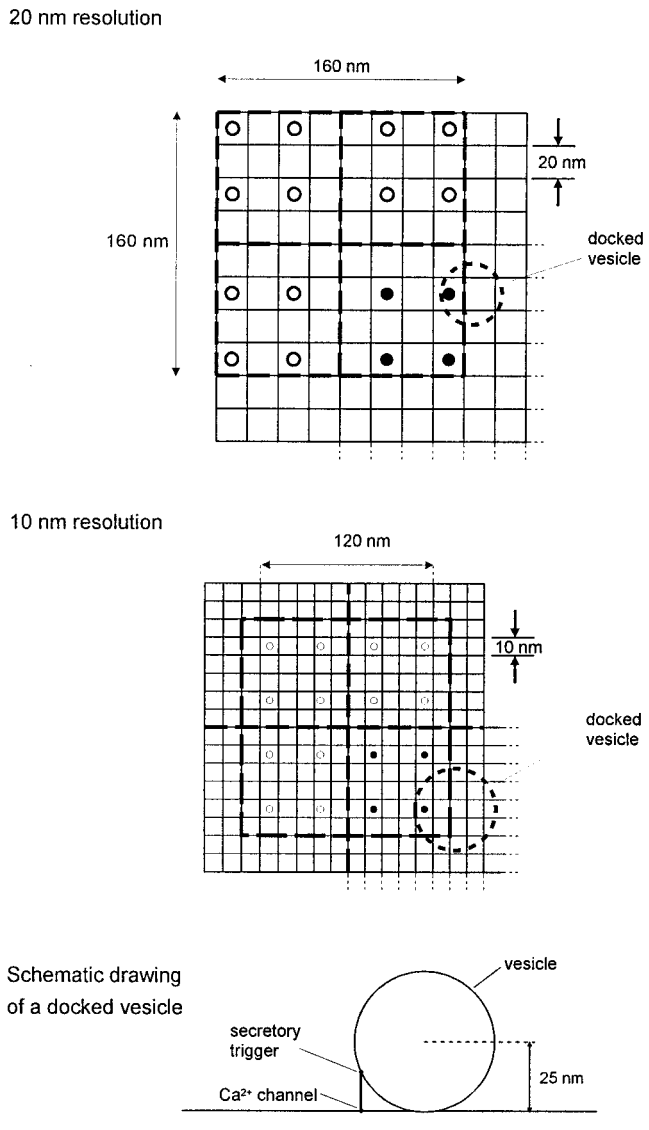

FIGURE 5 Disposition of open calcium channels during an action potential in an active zone, using 20- and 10-nm resolution geometries. The relationship between a docked vesicle, nearest calcium channel, and secretory trigger is also sketched.

cytoplasmic calcium buffering (Gabso et al., 1997) where the buffer mixture results in an effective buffer diffusion constant of 14 $\mu m^2\ s^{-1}$. The effective binding ratio κ_e (ratio of bound to free calcium) has been estimated to be 500 in crayfish nerve terminals (Tank et al., 1995). For the stationary buffer B_s we chose a K_d of 16 μM, a little less than that measured for the higher ionic strength of marine axoplasm (Alemà et al., 1973); for the mobile buffer B_m we assumed a K_d of 2 μM, twice the estimate for the mobile buffer found in mammalian hair cells (Roberts, 1994) and a diffusion coefficient of $D_m = 50\ \mu m^2\ s^{-1}$, based on aqueous measurements of calbindin (Feher et al., 1989) reduced by a tortuosity factor of 2.5 (Nowycky and Pinter, 1993); the diffusion coefficient for calcium was $D_{calcium} = 223\ \mu m^2\ s^{-1}$ (Allbritton et al., 1992).

Using the equations of Gabso et al. (1997):

$$\kappa \approx [B]_T/K_d,$$

assuming $[Ca^{2+}] < K_d$, where κ is the buffer ratio for either fixed (κ_s) or mobile (κ_m) buffer;

$$\kappa_e = \kappa_s + \kappa_m = 500,$$

$$D_e = D_m \cdot \kappa_m/(\kappa_s + \kappa_m),$$

where D_e is the effective diffusion constant for the buffer mixture, set to 14 $\mu m^2\ s^{-1}$ (Gabso et al., 1997). It follows that

$$[B_m]_T = 280\ \mu M, \quad \kappa_m = 140,$$

$$[B_s]_T = 5.76\ mM, \quad \kappa_s = 360.$$

The on-rates of the fixed and mobile buffer(s) were chosen to be $k_{on} = 1 \times 10^8\ M^{-1}\ s^{-1}$ (Xu et al., 1997). Each off-rate can be calculated from $k_{off} = K_d \cdot k_{on}$. Simulations of effects of fura-2 injection used the following parameters:

$K_d = 360$ nM (see Experimental Procedures),

$D_f = 118\ \mu m^2\ s^{-1}$ (Gabso et al., 1997),

$[B_f]_T = 400\ \mu M$,

$k_{on} = 2.7 \times 10^8\ M^{-1}\ s^{-1}$ (Kao and Tsien, 1988; value adjusted for $K_d = 360$ nM),

$k_{off} = 96.7\ s^{-1}$.

Calcium was extruded at the front and the rear surfaces of the bouton by a pump from a well-stirred layer (diffusion and binding are faster than pumping), represented by:

$$P = V/(\tau \cdot S) \cdot \kappa_e$$

To get an extrusion time constant τ of 5 s (Tank et al., 1995), with bouton volume $V = 2.56 \times 10^{-18}\ m^3$, pumping surfaces $S = 5.12 \times 10^{-12}\ m^2$, and a buffer ratio κ_e of 500, we use a pump rate of 50 $\mu m\ s^{-1}$.

We have shown experimentally that action potentials elevate $[Ca^{2+}]_i$ in presynaptic boutons containing 400 μM fura-2 by ~9 nM. We calculated the global increase in $[Ca^{2+}]_i$ to an action potential in our simulations including 400 μM fura-2 buffer to be 8.8 nM, similar to what is observed. Leaving fura-2 out of the simulation predicts a global rise in $[Ca^{2+}]_i$ of 28 nM in a presynaptic bouton.

Stage 2 reaction schemes

$[Ca^{2+}]_i$ transients sampled at various positions corresponding to possible receptor locations are the input for the second stage of modeling. These $[Ca^{2+}]_i$ transients drive calcium-receptor binding to generate transmitter release. Transmission at crayfish junctions depends on the third to fourth power $[Ca^{2+}]_i$ (Landò and Zucker, 1994), suggesting that multiple calcium ions bind stoichiometrically to the release machinery to trigger neurosecretion. In preliminary simulations we extended the previous finding (Yamada and Zucker, 1992) that very little facilitation is predicted by a scheme of multiple calcium ions binding to a single fast low-affinity class of receptor located 10–20 nm from the nearest calcium channel. We therefore adopted the reaction scheme of Yamada and Zucker (1992), which includes two classes of calcium binding sites (X) and (Y), but with three changes: 1) the number of calcium ions binding to X and Y sites was allowed to vary, 2) the facilitation site was endowed with kinetics fast enough to be consistent with results of Kamiya and Zucker (1994), and 3) the two sites to which calcium binds, X and Y, were spatially segregated. Site X is a very fast low-affinity site close to a calcium channel that we will call the secretory trigger, and site Y is a higher-affinity site at an uncertain location that we will call the facilitation site. We have explored schemes with one calcium ion binding to the facilitation site and three ions binding the secretory trigger, and with two calcium ions binding at each site. We denote the first scheme the X3Y1 model, and the second scheme the X2Y2 model.

In order to account for depression of transmitter release to repeated activation, secretion is often conceived as a sequential process in which vesicles move from a depot pool to a readily releasable or docked vesicle pool (Heinemann et al., 1993). However, no depression is observed to brief trains at crayfish junctions (Zucker, 1974), so a simpler model was used where X and Y represent secretory trigger and facilitation sites affecting release by a population of rapidly replenishable vesicles.

The X3Y1 model requires the binding of three calcium ions to X and one to Y before formation of a release promoter (R) whose concentration governs rate of transmitter release with kinetics limited by an inactivation process leading to a state (I) from which transmission is no longer possible, corresponding to vesicles which have fused and

released their contents:

$$\text{secretory trigger}$$
$$X + C \underset{k_{off}}{\overset{3k_{on}}{\rightleftharpoons}} CX + C \underset{2k_{off}}{\overset{2k_{on}}{\rightleftharpoons}} C_2X + C \underset{3k_{off}}{\overset{k_{on}}{\rightleftharpoons}} C_3X$$

$$\text{facilitation site} \qquad C + Y \underset{k_{off}}{\overset{k_{on}}{\rightleftharpoons}} CY$$

$$\text{release} \qquad C_3X + CY \overset{k_2}{\rightarrow} R \overset{k_3}{\rightarrow} I$$

The X2Y2 model used the following reaction scheme:

$$\text{secretory trigger}$$
$$X + C \underset{k_{off}}{\overset{2k_{on}}{\rightleftharpoons}} CX + C \underset{2k_{off}}{\overset{k_{on}}{\rightleftharpoons}} C_2X$$

$$\text{facilitation site}$$
$$Y + C \underset{k_{off}}{\overset{2k_{on}}{\rightleftharpoons}} CY + C \underset{2k_{off}}{\overset{k_{on}}{\rightleftharpoons}} C_2Y$$

$$\text{release}$$
$$C_2X + C_2Y \overset{k_2}{\rightarrow} R \overset{k_3}{\rightarrow} I$$

Predictions of these schemes were obtained by solving a system of first-order differential equations representing each of the reactions shown. We used $k_{on} = 5 \times 10^8$ M^{-1} s^{-1} for the secretory trigger (X sites; Zucker, 1994) and a $K_d = 200$ μM for their affinity (Yamada and Zucker, 1992). Substantial facilitation is activated at submicromolar levels of $[Ca^{2+}]_i$ (see above), and a site with 2–4 μM calcium affinity has been seen at crayfish neuromuscular junctions to regulate asynchronous release of transmitter between action potentials during a period when facilitation is also activated (Ravin et al., 1997). Inasmuch as this might reflect the action of calcium at facilitation (Y) sites, we chose a K_d of 3 μM for these sites. Rapid reduction of calcium buffering by photolysis of diazo-2 reduces facilitation within 10 ms or less (Kamiya and Zucker, 1994), indicating that facilitation is caused by calcium acting at a site with an off-rate faster than 100 s^{-1}. To be consistent with these results we chose a k_{off} of at least 100 s^{-1} for Y sites. Typical kinetics of vesicle fusion and transmitter release were generated by using $k_2 = 1$ M^{-1} ms^{-1} and $k_3 = 0.01$ μs^{-1} (Yamada and Zucker, 1992). EJP amplitude is taken as proportional to the maximal rate of transmitter release, or concentration of *R*.

Growth of facilitation

We first explored the behavior of the X3Y1 scheme with three calcium ions binding to the secretory trigger and one binding at the facilitation site. Our best fit to experimental data was obtained with the following parameter set: The facilitation site was located 100 nm below a calcium channel mouth, and had a K_d of 3 μM and a $k_{on} = 1.851 \times 10^8$ M^{-1} s^{-1}. We call this the spatial segregation model, because the two receptors in this model, the secretory trigger and the facilitation site, are located at different places in the active zone, and are therefore driven by different calcium transients.

If $[Ca^{2+}]$ changes abruptly, a new state of occupancy of a calcium binding site is reached with time constant τ, determined by the k_{on} and k_{off}, and by the new level of $[Ca^{2+}]$, where $\tau = 1/(k_{off} + k_{on}[Ca^{2+}])$. Table 2 shows the on-rates and off-rates of the facilitation site for different dissociation constants while keeping constant the kinetics of binding, τ, and the location of the facilitation site. The $[Ca^{2+}]$ predicted at the facilitation site at the end of a train from stage 1 (i.e., 5 μM) was used in calculating τ. The effects of varying K_d are summarized in Fig. 6 *A*. Facilitation of the fifth pulse in a 100-Hz tetanus decreases slightly on reducing K_d. However, this effect was minor compared to the effects of changing location or time constant of the facilitation site.

The effects of varying τ (while keeping K_d and location of the facilitation site constant) are summarized in Fig. 6 *B*. The strong dependence of facilitation on τ could underlie the dramatic difference in facilitation between proximal and central fibers of the opener muscle (Atwood, 1976). The facilitation site acts like a low-pass filter that integrates the effect of the calcium transient. Table 3 shows the on-rates and off-rates used for different time constants while keeping K_d constant.

Next we illustrate the dependence of facilitation on the location of the facilitation site at different distances (40–120 nm) below the calcium channel nearest the vesicle, and the effect of introducing an exogenous mobile buffer. Facilitation of the fifth pulse of the facilitation site ($k_{on} = 1.85 \times 10^8$ M^{-1} s^{-1}, $k_{off} = 555$ s^{-1}) below the channel mouth in the presence and in the absence of 400 μM fura-2 are summarized in Fig. 6 *C*. Facilitation depends strongly on the distance of the facilitation site from the channel mouth. However, the effect of adding fura-2 on facilitation was nearly independent of the facilitation site location: fura-2 always reduced facilitation by 50%. Results with the facilitation site located 80 nm lateral to the nearest calcium channel were virtually indistinguishable from those with site Y located 100 nm below the channel (Schlumpberger, 1999). The reason for this is that moving laterally from the

TABLE 2 Parameters explored with variable dissociation constant of the facilitation site but invariant time constant for $[Ca^{2+}] = 5$ μM

k_{on} (M^{-1} s^{-1})	k_{off} (s^{-1})	K_d (μM)	τ (ms)
2.469×10^8	246	1	0.675
1.851×10^8	555	3	0.675
1.347×10^8	808	6	0.675
9.876×10^7	987	10	0.675

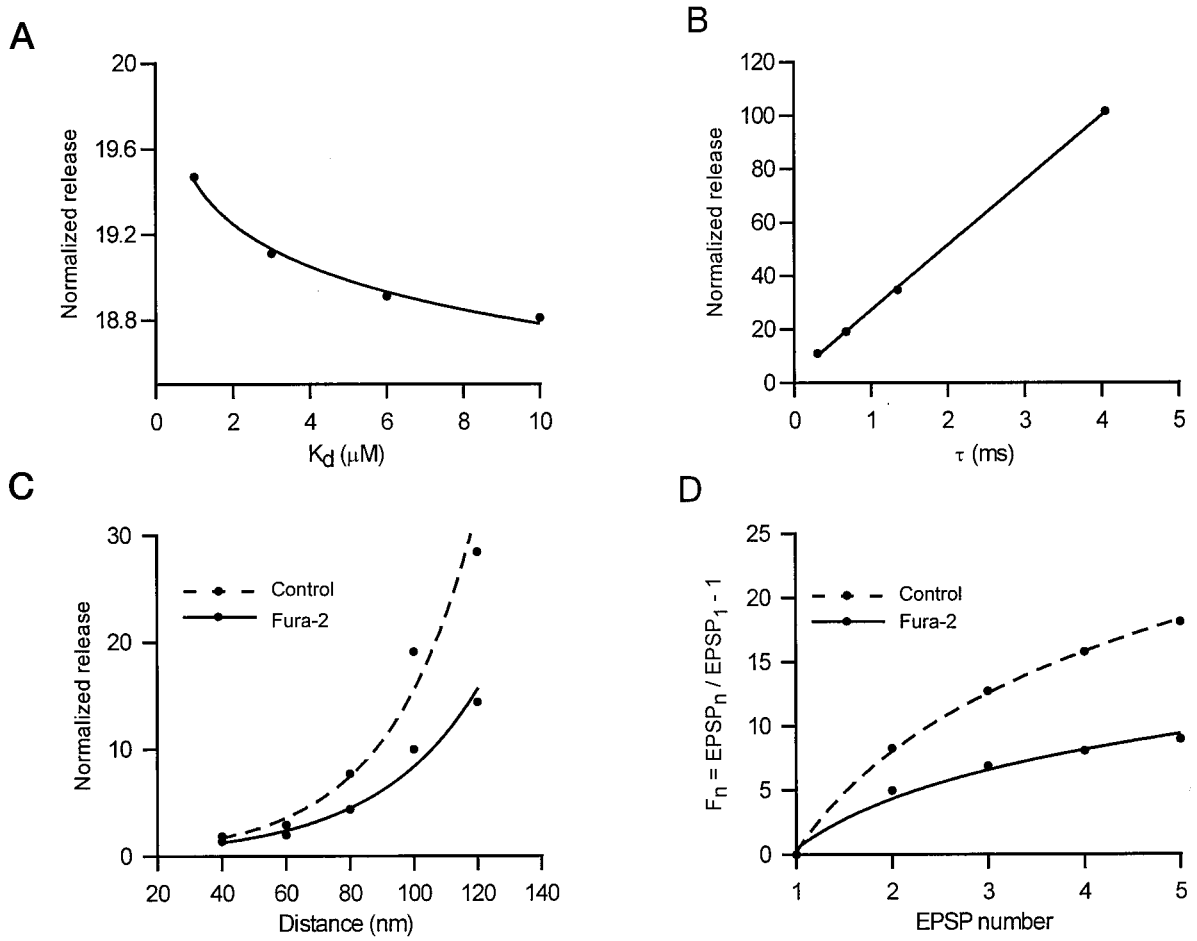

FIGURE 6 Effects of parameter variations in simulations of facilitation using the X3Y1 spatial segregation model. (*A*) Release by the fifth pulse at 100 Hz, normalized to release of the first pulse to show facilitation as a function of the dissociation constant of the facilitation site located 100 nm below the nearest calcium channel. The time constant of the facilitation site was 0.675 ms. Values were fitted to an exponential curve. (*B*) Normalized release of the fifth pulse as a function of different time constants of the facilitation site, with a dissociation constant of 3 μM. (*C*) Normalized release of the fifth pulse as a function of distance of the facilitation site to the calcium channel. Calcium transients were computed for the control situation (absence of fura-2) and after adding fura-2. Values were fitted to an exponential curve. (*D*) Accumulation of facilitation in a five-pulse 100-Hz train in the absence and presence of fura-2. The secretory trigger was 20 nm away from the nearest calcium channel and the facilitation site was 100 nm below the calcium channel. On-rate of the facilitation site was 1.85×10^8 M^{-1} s^{-1}, off-rate 555 s^{-1}.

outermost calcium channel puts the facilitation site further from the other channels in the active zone than moving deeper into the cytoplasm below the membrane.

Simulations up to this point used 20-nm submembrane compartments and a 20-nm distance from secretory trigger to nearest calcium channel mouth. We have also explored the effects of using a finer spatial resolution grid (10 nm), with somewhat smaller active zones and higher calcium channel density (see Stage 1 Diffusion Parameters above). $[Ca^{2+}]_i$ peaks reached 76 and 95 μM at the secretory trigger in the first and fifth pulses using 20-nm resolution, rising to 84 and 107 μM with the 10-nm resolution and more compact active zone. When the secretory trigger was moved to 10 nm from the nearest calcium channel, $[Ca^{2+}]_i$ peaks grew to 139 and 162 μM during first and last pulses. However, the $[Ca^{2+}]_i$ peaks reached by the first and last pulses at the facilitation site changed only a few percent, regardless of the resolution and active zone configuration used. Consequently, the magnitude of facilitation reached by the fifth pulse was affected by $<8\%$ when resolution and active zone configuration or distance to secretory trigger were changed. Simulations with fura-2 were similarly affected, so that the reduction in facilitation by fura-2 was

TABLE 3 Parameters explored with variable facilitation time constant but invariant dissociation constant ($[Ca^{2+}] = 5$ μM)

k_{on} (M^{-1} s^{-1})	k_{off} (s^{-1})	K_d (μM)	τ (ms)
4.166×10^8	1250	3	0.300
1.851×10^8	555	3	0.675
9.259×10^7	277	3	1.35
3.086×10^7	92.6	3	4.05

virtually independent of these alternative parameter choices. Details of these simulations may be found in Schlumpberger (1999).

Fig. 6 *D* shows the growth of facilitation in the presence and absence of fura-2 with the Y site located 100 nm below the calcium channel using the 20-nm resolution and active zone configuration. No other parameter set could fit experimentally observed data as well. The response to the fifth pulse in the control simulation showed a facilitation of 18.1, while facilitation of 8.99 was observed in the fura-2 simulation. Transmission in the presence of fura-2 was reduced by 43.7%, similar to our experimental value of 57 ± 19%. These results with the first and fifth pulses are very similar to those observed experimentally (see first section of Results and Fig. 2 *C*). The X3Y1 model thus accounts well for the magnitude of facilitation and the effects of mobile exogenous buffers on facilitation and transmission. It is important to note that a high-affinity facilitation site located in close proximity to a channel mouth is saturated by the calcium entering in each action potential, and therefore cannot produce facilitation (Fig. 6 *C*). Spatially segregating the facilitation site and the secretory trigger was the only way to prevent that saturation and produce facilitation using a facilitation site with sufficiently high affinity and fast kinetics to be consistent with experimental findings (Kamiya and Zucker, 1994; Ravin et al., 1997).

One failure of these simulations is that they did not describe the growth of facilitation observed experimentally: real EJPs grow in an accelerating fashion, whereas model responses grow along a much shallower curve (cf. Figs. 2 *C* and 6 *D*). The shape of this growth curve for model data was virtually identical throughout the entire parameter space. The accelerating tetanic accumulation of real facilitation suggests the possibility of cooperative calcium binding in activating facilitation. The X2Y2 model is a simple formulation of such a possibility. However, simulations of this scheme throughout the same parameter space as for the X3Y1 scheme were no more successful in replicating the shape of the growth of tetanic facilitation (data not shown, see Schlumpberger, 1999). Moreover, the X2Y2 scheme resulted in too large a reduction in facilitation (to 25%) in the presence of exogenous buffer, and was therefore less successful than the X3Y1 scheme in predicting experimental results.

Delaney et al. (1991) showed that presynaptic injection of EGTA reliably reduced facilitation without consistent effect on basal transmission, unlike BAPTA and fura-2, which in our present experiments consistently reduce transmission and facilitation about equally. We simulated EGTA injection by replacing fura-2 with 2 mM of a mobile buffer with $k_{on} = 2.7 \times 10^6\ M^{-1}\ s^{-1}$ and $k_{off} = 0.5\ s^{-1}$ (Naraghi, 1997); simulated facilitation was reduced by 23%, while simulated transmission was reduced by only 4%.

Decay of facilitation

We investigated whether our buffered calcium diffusion model and X3Y1 reaction scheme could also account for the decay of facilitation. We simulated our experimental measurements by calculating the spatiotemporal $[Ca^{2+}]_i$ pattern for 1300 ms after the 30-ms conditioning tetanus of four pulses at 100 Hz, saving all state variables (calcium concentration, exogenous and endogenous mobile buffer, and endogenous immobile buffer for each compartment) at various intervals after the end of the tetanus. We used the state variables at these intervals as initial conditions to calculate responses to test pulses, and transmitter release was computed using the X3Y1 scheme with the parameter choices determined above from fitting simulations to the growth of facilitation. The simulated decay of facilitation with and without fura-2 is shown in Fig. 3, *C* and *D*, along with the closest fitting two-exponential decay curves like those used to fit experimental data. Parameters for the exponentials are given in Table 4.

The simulated decay of facilitation resembled the form of experimental results (Fig. 3), and parameters of the two exponential components fell within the range of observed values (Tables 1 and 4). The simulated effects of exogenous buffer (shown in parentheses) were also similar to the experimental results: 26% (33%) reduction in F_1, 34% (35%) reduction in τ_1, 41% (32%) reduction in F_2, and 32% (53%) reduction in τ_2.

In our model, the two components of facilitation both arise from diffusional dissipation of $[Ca^{2+}]_i$ at the facilitation site; the first component is also influenced by desaturation of calcium buffers in the region of the facilitation site. The intrinsic rate of decay of facilitation depends on $[Ca^{2+}]_i$, and from experimental evidence is faster than 10 ms, and in our model is ≤2 ms. Even the fastest component of facilitation is slower than this.

Calcium dependence of facilitation and secretion

Transmission depends on the concentration of calcium in the external medium ($[Ca^{2+}]_e$) raised to the third to fourth power (Dudel, 1981, 1989a), while facilitation is much less sensitive to $[Ca^{2+}]_e$. We tested our model's ability to predict these results by assuming a linear relationship between calcium influx and $[Ca^{2+}]_e$, and observing the effects of reducing single channel influx by 50%. Fig. 7 *A* shows simulated calcium transients at a secretory trigger 20 nm from the nearest calcium channel, and Fig. 7 *B* depicts calcium transients at a facilitation site 100 nm below the

TABLE 4 Simulated decay of facilitation

	F_1	τ_1 (ms)	F_2	τ_2 (ms)	Plateau
Control	30.1	13.0	4.1	359.9	0
Fura-2	20.3	8.4	2.8	169.0	0

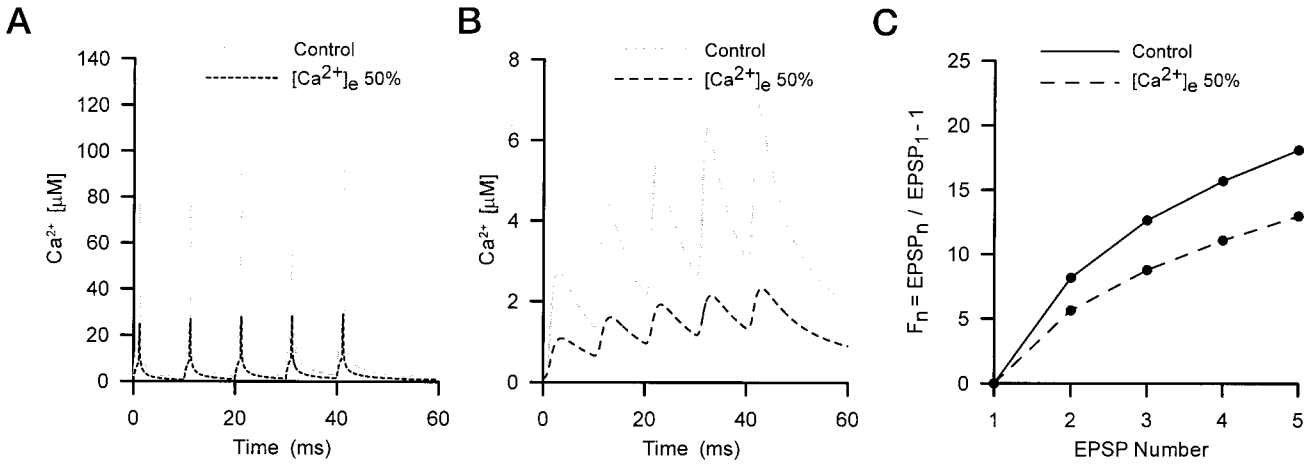

FIGURE 7 Effects of changing external calcium concentration. Dependence of $[Ca^{2+}]_i$ at the secretory trigger (*A*) and the facilitation site (*B*) on $[Ca^{2+}]_e$. (*C*) The effect of reducing $[Ca^{2+}]_e$ by 50% on facilitation.

nearest calcium channel. In both cases, reducing influx to half leads to even more reduced peak $[Ca^{2+}]_i$ transients, due to desaturation of endogenous calcium buffers. This results in a very large reduction in the predicted amplitude of a single EJP, to 4% of its amplitude in normal $[Ca^{2+}]_e$, which corresponds to a 4.6-power dependence of transmission on $[Ca^{2+}]_e$, similar to the highest values observed experimentally (Dudel, 1981, 1989a). Fig. 7 *C* shows that facilitation to the second through fifth pulses was reduced by only 28–31%, for a 50% reduction in $[Ca^{2+}]_e$. This may be compared to the roughly 50% reduction in two-pulse facilitation observed by Dudel (1989b) when $[Ca^{2+}]_e$ was reduced by 80%.

Monte Carlo simulations

Our results suggest that facilitation could be caused by a single calcium ion binding to a target molecule located ~100 nm away from the nearest calcium channel mouth. Because this is greater than a synaptic vesicle diameter, it seemed physiologically unrealistic, although not inconceivable. Alternatively, it seemed possible that the facilitation target is actually much closer to a calcium channel mouth, but that diffusion to this target is restricted or obstructed, so that the time taken to reach this nearby target would be the same as for unrestricted free diffusion to a distance of ~100 nm.

We envision at least two possible scenarios (Fig. 8 *A*): 1) the facilitation site might be located in a hard-to-reach vestibule on the back of a docking complex, which consists of a dense protein conglomerate surrounding the vesicle-membrane contact region; and 2) and it might be located at the top of the vesicle, where it attaches to cytoskeletal elements that might control the vesicle's availability for release. In either case, the vesicle and the docking complex are impermeable to calcium ions and represent diffusion barriers that would obstruct its movements. We used Monte Carlo Random Walk simulations to explore the effects of such barriers on the diffusion of calcium ions from the channel mouth to the facilitation target.

In the first scenario, random walks were conducted from the calcium channel mouth in the cell membrane (also impermeable) located 20 nm from the center of the docking complex (8 nm from the nearest point), to a facilitation binding site at the back of a cylindrical vestibule—10 nm in radius and 4 nm high—within the docking complex at the end of a 2-nm long, 1 × 4-nm wide tunnel at the back of the docking complex facing away from the nearest channel mouth. The target was regarded as absorbing, and repeated bindings were not allowed. A histogram of frequency of hits on the facilitation target versus numbers of steps in the walk, corresponding to $[Ca^{2+}]_i$ at the target versus time, was constructed for multiple walks. This was compared to control simulations, consisting of random walks to an unobstructed target located 100 nm below the plasma membrane.

Diffusion to the unobstructed site in semi-infinite space at a distance of 100 nm occurred with an average time of 405 μs. For diffusion around the docking complex, Fig. 8 *B* shows that the putative facilitation site was reached after an average delay of 399 μs. The histograms are similar, reflecting a similar time course of residual calcium at a restricted site behind the docking complex and at an unrestricted cytoplasmic location 100 nm away from a calcium channel.

The second scenario was modeled by random walks to a facilitation site on the back of the vesicle facing the interior cytoplasm. Diffusion around the vesicle to this location (Fig. 8 *C*) occurred with an average delay of 426 μs. This is comparable to unrestricted diffusion to a target located at 100 nm (average delay 364 μs). The two control simulations

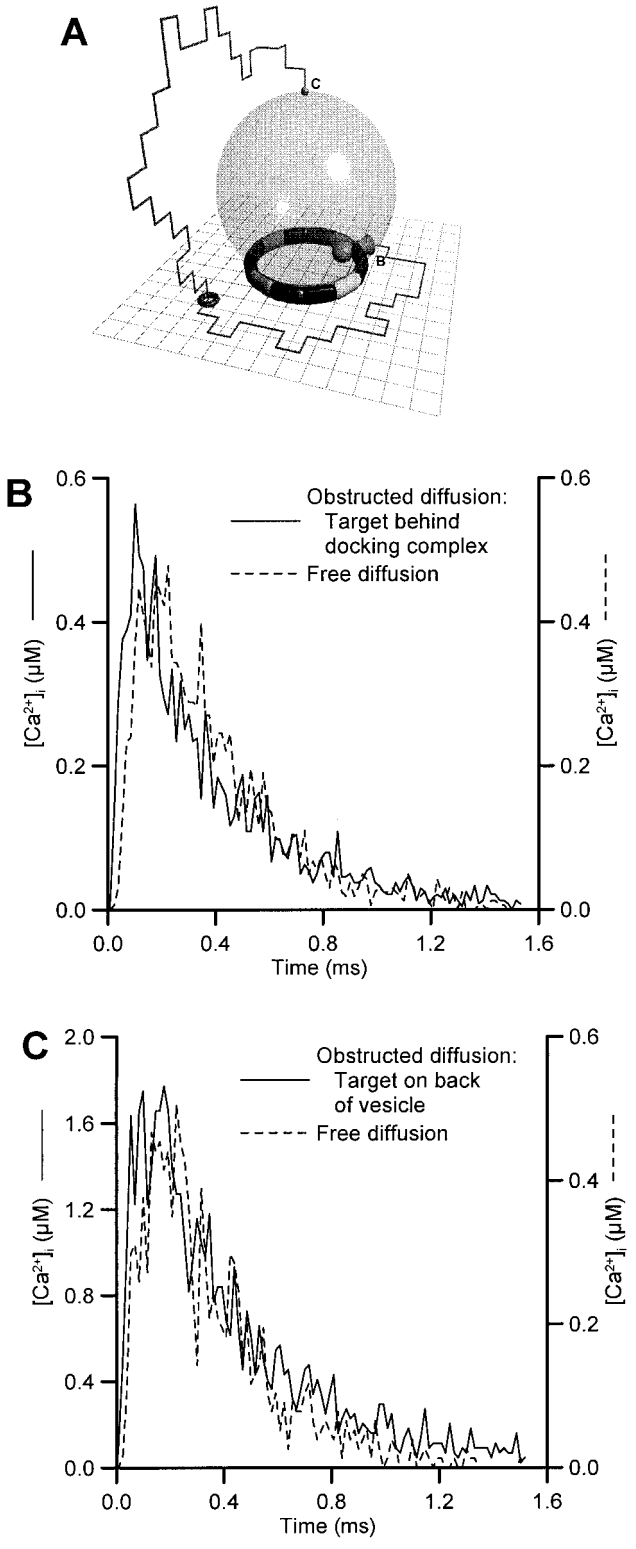

FIGURE 8 Monte Carlo simulations of restricted diffusion. (*A*) Cartoon showing simplified random walks from a calcium channel mouth to a putative facilitation site within a vestibule inside the docking complex (*B*) or on the back of a docked vesicle (*C*). The vestibule containing the facilitation site is not drawn to scale. (*B*) Random walk simulations of diffusion to a buried site accessible from the back of the docking complex (*solid line*), compared to free diffusion to a site 100 nm below the channel mouth (*dashed line*). Bin width is 1000 steps. (*C*) Simulated diffusion to an obstructed site on the back of a vesicle, compared to free diffusion to an unobstructed site at 100 nm.

(average delays of 405 and 364 μs) give an indication of the variability observed on repeated simulation runs. The profiles of residual calcium at a putative facilitation site on the back of a synaptic vesicle and 100 nm away from a calcium channel in open cytoplasm are similar. The higher predicted $[Ca^{2+}]_i$ at the back of the vesicle is due to the effects of neighboring vesicles and associated calcium channels.

DISCUSSION

Our results and conclusions may be summarized as follows:

1. We measured a residual calcium in inhibitory nerve terminals accumulating during a brief tetanus of ~9 nM per action potential. Facilitation in these terminals resembled that of excitatory terminals where it can be more accurately characterized;
2. Facilitation in excitatory terminals was reduced and its decay accelerated by exogenous presynaptic calcium buffers;
3. Simulations of calcium influx, buffering, diffusion, and extrusion predicted the observed level of residual calcium concentration;
4. Simulations failed to generate facilitation due to calcium binding to a single low-affinity secretory trigger, or with a separate high-affinity facilitation site located near calcium channels;
5. The simulated spatiotemporal profile of $[Ca^{2+}]_i$ acting on a secretory trigger 10–20 nm from the nearest channel mouth and on a high-affinity facilitation site 100 nm below or 80 nm to one side predicted a magnitude of facilitation in a train and kinetics of decay of facilitation matching experimental observations; however, the time course of growth of facilitation in a train was not accurately predicted. This site might correspond to a restricted location behind the vesicle docking complex or at the back of a vesicle;
6. Observed effects of changes in $[Ca^{2+}]_e$, and of known levels of exogenous buffer, on amplitude of transmission and magnitude and kinetics of facilitation were well-predicted by simulations.

Comparison to other experimental work

We estimate that ~90 calcium channels open in a bouton during an action potential (16 per active zone times 6 active zones per hemisphere of bouton facing a muscle fiber). Tank et al. (1995) estimated that ~450 channels opened in an action potential. Most of the difference is due to the fact that their calculations are based on a bouton diameter (5

μm) 67% larger than ours, accounting for a 2.8-fold larger channel number. Moreover, we assume a larger single channel current—2.27×10^{-21} moles including tail current versus 1.35×10^{21} moles in Tank et al. (1995) ignoring tail current—as well as a slightly lower endogenous buffer ratio (500 instead of 600), which together contribute another factor of 2 to the difference in estimates of open channel number. Tank et al. (1995) estimate 50 channels per active zone (compared to our 16), largely because they assume a higher active zone density than we do; our estimates are based on more recent ultrastructural measurements (Cooper et al., 1995).

Our results on crayfish are consistent with earlier measurements of the characteristics of facilitation (Zucker, 1974) and effects of some authors (Hochner et al., 1991), but not others (Winslow et al., 1994) using exogenous buffer. We are uncertain why the latter group observed no effect of BAPTA-AM on facilitation, but we note that loading of acetoxymethyl ester buffers is vicarious and final buffer levels are uncertain, which is why we turned to loading with fura-2 whose presynaptic concentration can be measured fluorometrically.

Many authors (Zucker, 1994, 1999) report a correlation between residual calcium and facilitation, and Delaney et al. (1989) found that presynaptic EGTA injection reduced facilitation, in agreement with our present results. Atluri and Regehr (1996) also found that exogenous buffer reduces facilitation and speeds its decay in cerebellar synapses. Blundon et al. (1993) used effects of BK-type calcium-activated potassium current ($I_{K(Ca)}$) on membrane resistance to estimate the time course of residual calcium in crayfish motor nerve terminals after depolarizing pulses and concluded that residual calcium dissipated much more rapidly than facilitation, and therefore was not responsible for its generation. However, $I_{K(Ca)}$ is exquisitely sensitive to membrane potential (Hille, 1992), and the decay rates observed match the reported voltage-dependent relaxation of this current. Furthermore, BK-type potassium channels are colocalized in close proximity with calcium channels in vertebrate nerve terminals (Robitaille et al., 1993), and may therefore detect a local $[Ca^{2+}]_i$ closer to calcium channel mouths than at the facilitation trigger.

We were most successful in predicting effects of exogenous buffer on facilitation by assuming a linear relationship between facilitation and residual calcium at the appropriate location. Several recent experimental studies support this idea: Atluri and Regehr (1996, 1998) reported an apparently linear relation between facilitation and residual calcium at rat cerebellar synapses. Wright et al. (1996) reported an apparently linear relationship between calcium influx at crayfish nerve terminals and facilitation. Vyshedskiy and Lin (1997a) showed that facilitation to a conditioning pulse grew as the cube root of secretion to that pulse, again suggesting a linear dependence of facilitation on $[Ca^{2+}]_i$.

We also succeeded in predicting the maximal experimental values of the Hill coefficient of the dependence of transmission on $[Ca^{2+}]_e$ (Dudel, 1981, 1989a). Average measured values of the Hill coefficient are between 3 and 4, somewhat less than our simulated value of 4.6, but we would expect experimental estimates of this power dependence to be limited by the saturable (i.e., less than linear) dependence of calcium influx on $[Ca^{2+}]_e$ (Rubart et al., 1996).

Our failure to accurately predict growth of facilitation might result from a number of factors:

First, parameters of stage 1 modeling—the spatiotemporal $[Ca^{2+}]_i$ pattern: Although all our parameter choices were based on experimental values, few came from measurements of crayfish neuromuscular junctions. Values for the affinities, kinetics, diffusibilities, and assumed homogeneity of endogenous buffers, the assumed tortuosity, and the single channel current all came from other preparations, and extrapolation to crayfish is uncertain.

Second, geometrical considerations: active zones are actually crowded with vesicles, fusion, docking and cytoskeletal proteins, and organelles like mitochondria and presynaptic dense bodies, which can have a significant impact on diffusion of calcium and buffers. Such physical obstructions could lead to complex and anomalous effects on diffusion (Saxton, 1994; Ölveczky and Verkman, 1998; Kits et al., 1999), significantly altering the spatiotemporal $[Ca^{2+}]_i$ profile, in particular in the region of the site causing facilitation.

Finally, secretion-facilitation reaction schemes: we simulated only the simplest reaction schemes consistent with present evidence. More complex alternatives, involving positive or negative cooperativity at the secretory or facilitation calcium binding sites, allosteric interactions between the two calcium binding sites, etc., were not considered.

The possible space of alternative parameter values, and of reaction schemes, is enormous, and its exploration is impractical when such intensive computation is involved. We do not know which one of these assumptions is responsible for the imperfect prediction of accumulation of facilitation.

Spatial segregation of secretory trigger and facilitation sites

Our simulations placed the secretory trigger at 10–20 nm from a calcium channel, and the facilitation site 80–100 nm away. Synaptotagmin I is currently the most popular candidate for the secretory trigger (Bennett, 1997). Interactions between synaptotagmin, syntaxin, and calcium channels are consistent with separation distances of $<$20 nm, and we chose K_d of 200 μM for the calcium affinity of the secretory trigger because this is similar to synaptotagmin's affinity for calcium in affecting syntaxin binding.

The identity of molecules mediating calcium's activation of facilitation is unknown. The 80–100-nm distance from the calcium channel required for our simulations to generate

facilitation of appropriate magnitude suggests a target rather distant from the presynaptic membrane. Monte Carlo random walk simulations suggest that one possibility consistent with an approximate diffusion distance of 100 nm is that calcium acts at the back surface of docked vesicles, perhaps to alter cytoskeletal-vesicle interactions mediated by a protein such as scinderin (Zhang et al., 1996). In this scenario, transmitter release requires both the action of calcium at a release trigger and at a site that "primes" vesicles, making them fully available for release.

Additional Monte Carlo simulations suggest the alternative possibility that calcium acts at a facilitation site with restrictive access on the back of the docking complex facing away from the nearest calcium channel. Such a docking site could act locally in concert with the secretory trigger, either to "prime" vesicles for release or to alter the probability of release of already fully docked vesicles. Observations that facilitation is accompanied by an increase in the early rate of release, but not the maximum rate of release, following an action potential (Vyshedskiy and Lin, 1997b) appear consistent with either local interaction between the facilitation site and secretory trigger or priming of vesicles for release.

Alternative approaches to modeling calcium diffusion

Our calculations of the spatiotemporal $[Ca^{2+}]_i$ profiles during repetitive stimulation use numerical solutions of the differential equations describing diffusion, buffering, and extrusion, which is similar to the approach in some previous simulations (Yamada and Zucker, 1992; Winslow et al., 1994; Cooper et al., 1996), although we used more complex assumptions about the nature of endogenous buffering based on recent measurements. A number of other studies of calcium diffusion have introduced approximations that greatly simplify the computational complexity of such problems. Wagner and Keizer (1994) showed that under the assumption of local buffer equilibrium, Ca^{2+} redistribution can be calculated by a single transport equation for Ca^{2+} that is very similar to the diffusion equation for a single species. This simplification, known as the rapid buffer approximation (RBA), reduces the computational load to calculate the calcium diffusion picture enormously (Neher, 1998), and has been used in several other simulation studies (e.g., Hovav et al., 1992; Bertram et al., 1999). The RBA is valid only when $\tau_{buffering} \ll \tau_{diffusion}$, meaning that buffering must be much faster than diffusion. The buffering time scale can be estimated by

$$\tau_{buffering} = 1/(k_{off} + k_{on}([Ca^{2+}] + [B])),$$

while the characteristic time for diffusion (with L as a length characteristic of the spatial profile) can be written as $\tau_{diffusion} = L^2/D_{calcium}$. In our case for a 100 μM Ca^{2+} spike with the dominant immobile buffer ([B] = 5.76 mM, $k_{on} = 1.8 \times 10^8\ M^{-1}\ s^{-1}$, $k_{off} = 555\ s^{-1}$), $\tau_{buffering}$ would be 0.95 μs, and the time for a calcium ion to diffuse 20 nm from the channel mouth would be 1.79 μs, while for a 10-nm separation between channel mouth and secretory target $\tau_{diffusion} = 0.45$ μs. The criterion for application of the RBA is not satisfied; its application would seriously distort $[Ca^{2+}]_i$ estimates at the secretory trigger. Moreover, the RBA requires that calcium buffers be non-saturable, while our simulations show that the $[Ca^{2+}]_i$ transients near the secretory trigger produce substantial saturation of both mobile and immobile cytoplasmic buffers (Schlumpberger, 1999).

Naraghi and Neher (1997), Neher (1998), and Bertram et al. (1999) explore linear approximations to the buffer equations when $[Ca^{2+}]_i$ transients are small and buffer saturation is avoided, and produce a relatively simple expression for the steady-state level of $[Ca^{2+}]_i$ reached in close proximity to calcium channel mouths. These approximations also do not apply in our case because of the large saturation of cytoplasmic buffers that actually occurs in the region separating a calcium channel from the secretory target (Schlumpberger, 1999). They are also not useful at longer distances from calcium channels, because equilibration is too slow compared to the duration of calcium influx to permit establishment of a steady state. For the same reason, we cannot make use of the simplifications introduced by Roberts (1994), using steady-state solutions to calculate $[Ca^{2+}]_i$ elevations in the immediate vicinity of calcium channels.

We thank Richard Ayer, Vahri Beaumont, Russell English, Harold Lecar, Edwin Lewis, Jen-Wei Lin, Greg Tomaschke, and Matthew Whim for technical help and comments.

This work was supported by National Institutes of Health Grant NS 15114, and grants of computer time on the San Diego Supercomputer Center Cray T90 computer from the National Partnership for Advanced Computational Infrastructure and on the Lawrence Livermore National Laboratory Cray T3D computer from the Advanced Computing Initiative in Science and Engineering. R.S.Z. was a Research Professor of the Miller Institute for Basic Research in Science.

REFERENCES

Adler, E. M., G. J. Augustine, S. N. Duffy, and M. P. Charlton. 1991. Alien intracellular calcium chelators attenuate neurotransmitter release at the squid giant synapse. *J. Neurosci.* 11:1496–1507.

Alemà, S., P. Calissano, G. Rusca, and A. Giuditta. 1973. Identification of a calcium-binding, brain specific protein in the axoplasm of squid giant axons. *J. Neurochem.* 20:681–689.

Allbritton, N. L., T. Meyer, and L. Stryer. 1992. Range of messenger action of calcium ion and inositol 1,4,5-trisphosphate. *Science.* 258: 1812–1815.

Atluri, P. P., and W. G. Regehr. 1996. Determinants of the time course of facilitation at the granule cell to Purkinje cell synapse. *J. Neurosci.* 16:5661–5671.

Atluri, P. P., and W. G. Regehr. 1998. Delayed release of neurotransmitter from cerebellar granule cells. *J. Neurosci.* 18:8214–8227.

Atwood, H. L. 1976. Organization and synaptic physiology of crustacean neuromuscular systems. *Prog. Neurobiol.* 7:291–391.

Bennett, M. K. 1997. Ca^{2+} and the regulation of neurotransmitter secretion. *Curr. Opin. Neurobiol.* 7:316–322.

Bertram, R., A. Sherman, and E. F. Stanley. 1996. Single-domain/bound calcium hypothesis of transmitter release and facilitation. *J. Neurophysiol.* 75:1919–1931.

Bertram, R., G. D. Smith, and A. Sherman. 1999. Modeling study of the effects of overlapping Ca^{2+} microdomains on neurotransmitter release. *Biophys. J.* 76:735–750.

Blundon, J. A., S. N. Wright, M. S. Brodwick, and G. D. Bittner. 1993. Residual free calcium is not responsible for facilitation of neurotransmitter release. *Proc. Natl. Acad. Sci. U.S.A.* 90:9388–9392.

Cooper, R. L., L. Marin, and H. L. Atwood. 1995. Synaptic differentiation of a single motor neuron: conjoint definition of transmitter release, presynaptic calcium signals, and ultrastructure. *J. Neurosci.* 15: 4209–4222.

Cooper, R. L., J. L. Winslow, C. K. Govind, and H. L. Atwood. 1996. Synaptic structural complexity as a factor enhancing probability of calcium-mediated transmitter release. *J. Neurophysiol.* 75:2451–2466.

Crank, J. 1975. The Mathematics of Diffusion. Oxford University Press, Oxford.

Delaney, K. R., and D. W. Tank. 1994. A quantitative measurement of the dependence of short-term synaptic enhancement on presynaptic residual calcium. *J. Neurosci.* 14:5885–5902.

Delaney, K., D. W. Tank, and R. S. Zucker. 1991. Presynaptic calcium and serotonin-mediated enhancement of transmitter release at crayfish neuromuscular junction. *J. Neurosci.* 11:2631–2643.

Delaney, K. R., R. S. Zucker, and D. W. Tank. 1989. Calcium in motor nerve terminals associated with posttetanic potentiation. *J. Neurosci.* 9:3558–3567.

Dudel, J. 1981. The effect of reduced calcium on quantal unit current and release at the crayfish neuromuscular junction. *Pflügers Arch.* 391: 35–40.

Dudel, J. 1989a. Calcium dependence of quantal release triggered by graded depolarization pulses to nerve terminals on crayfish and frog muscle. *Pflügers Arch.* 415:289–298.

Dudel, J. 1989b. Calcium and depolarization dependence of twin-pulse facilitation of synaptic release at nerve terminals of crayfish and frog muscle. *Pflügers Arch.* 415:304–309.

Feher, J. J., C. S. Fullmer, and G. K. Fritzsch. 1989. Comparison of the enhanced steady-state diffusion of calcium by calbindin-D9K and calmodulin: possible importance in intestinal calcium absorption. *Cell Calcium.* 10:189–203.

Fischer, T. M., R. S. Zucker, and T. J. Carew. 1997. Activity-dependent potentiation of synaptic transmission from L30 inhibitory interneurons of *Aplysia* depends on residual presynaptic Ca^{2+} but not on postsynaptic Ca^{2+}. *J. Neurophysiol.* 78:2061–2071.

Gabso, M., E. Neher, and M. E. Spira. 1997. Low mobility of the Ca^{2+} buffers in axons of cultured Aplysia neurons. *Neuron.* 18:473–481.

Grynkiewicz, G., M. Poenie, and R. Y. Tsien. 1985. A new generation of Ca^{2+} indicators with great improved fluorescence properties. *J. Biol. Chem.* 260:3440–3450.

Heidelberger, R., C. Heinemann, E. Neher, and G. Matthews. 1994. Calcium dependence of the rate of exocytosis in a synaptic terminal. *Nature.* 371:513–515.

Heinemann, C., L. von Rüden, R. H. Chow, and E. Neher. 1993. A two-step model of secretion control in neuroendocrine cells. *Pflügers Arch.* 424:105–112.

Hille, B. 1992. Ionic Channels of Excitable Membranes, 2nd Ed. Sinauer Associates, Sunderland, Massachusetts, 121–124.

Hochner, B., H. Parnas, and I. Parnas. 1991. Effects of intra-axonal injection of Ca^{2+} buffers on evoked release and on facilitation in the crayfish neuromuscular junction. *Neurosci. Lett.* 125:215–218.

Hovav, G., H. Parnas, and I. Parnas. 1992. Neurotransmitter release: facilitation and three-dimensional diffusion of intracellular calcium. *Bull. Math. Biol.* 54:875–894.

Kamiya, H., and R. S. Zucker. 1994. Residual calcium and short-term synaptic plasticity. *Nature.* 371:603–606.

Kao, J. P., and R. Y. Tsien. 1988. Ca^{2+} binding kinetics of fura-2 and azo-1 from temperature-jump relaxation measurement. *Biophys. J.* 53: 635–639.

Katz, B., and R. Miledi. 1968. The role of calcium in neuromuscular facilitation. *J. Physiol.* 195:481–492.

Kits, K. S., T. A. de Vlieger, B. W. Kooi, and H. D. Mansvelder. 1999. Diffusion barriers limit the effect of mobile calcium buffers on exocytosis of large dense cored vesicles. *Biophys. J.* 76:1693–1705.

Landò, L., and R. S. Zucker. 1994. Ca^{2+} cooperativity in neurosecretion measured using Ca^{2+} photolabile chelators. *J. Neurophysiol.* 72: 825–830.

Llinás, R., I. Z. Steinberg, and K. Walton. 1981. Relationship between presynaptic calcium current and postsynaptic potential in squid giant synapse. *Biophys. J.* 33:323–352.

Llinás, R., M. Sugimori, and R. B. Silver. 1992. Microdomains of high calcium concentration in a presynaptic terminal. *Science.* 256:677–679.

Martin, A. R. 1955. A further study of the statistical composition of the end-plate potential. *J. Physiol.* 130:114–122.

Mulkey, R. M., and R. S. Zucker. 1992. Posttetanic potentiation at the crayfish neuromuscular junction is dependent on both intracellular calcium and sodium ion accumulation. *J. Neurosci.* 12:4327–4336.

Naraghi, M. 1997. T-jump study of calcium binding kinetics of calcium chelators. *Cell Calcium.* 22:255–268.

Naraghi, M., and E. Neher. 1997. Linearized buffered Ca^{2+} diffusion in microdomains and its implications for calculation of $[Ca^{2+}]$ at the mouth of a calcium channel. *J. Neurosci.* 17:6961–6973.

Neher, E. 1998. Usefulness and limitations of linear approximations to the understanding of Ca^{++} signals. *Cell Calcium.* 24:345–357.

Nowycky, M. C., and M. J. Pinter. 1993. Time courses of calcium and calcium-bound buffers following calcium influx in a model cell. *Biophys. J.* 64:77–91.

Ölveczky, B. P., and A. S. Verkman. 1998. Monte Carlo analysis of obstructed diffusion in three dimensions: application to molecular diffusion in organelles. *Biophys. J.* 74:2722–2730.

Onodera, K., and A. Takeuchi. 1978. Effects of membrane potential and temperature on the excitatory post-synaptic current in the crayfish muscle. *J. Physiol.* 278:183–192.

Press, W. H., B. P. Flannery, S. A. Teukolsky, and W. T. Vetterling. 1988. Numerical Recipes in C. Cambridge University Press, Cambridge. 47–48.

Ravin, R., M. E. Spira, H. Parnas, and I. Parnas. 1997. Simultaneous measurement of intracellular Ca^{2+} and asynchronous transmitter release from the same crayfish bouton. *J. Physiol.* 501:251–262.

Roberts, W. M. 1994. Localization of calcium signals by a mobile calcium buffer in frog saccular hair cells. *J. Neurosci.* 14:3246–3262.

Robitaille, R., M. L. Garcia, G. J. Kaczorowski, and M. P. Charlton. 1993. Functional colocalization of calcium and calcium-gated potassium channels in control of transmitter release. *Neuron.* 11:645–655.

Rubart, M., J. B. Patlak, and M. T. Nelson. 1996. Ca^{2+} currents in cerebral artery smooth muscle cells of rat at physiological Ca^{2+} concentration. *J. Gen. Physiol.* 107:459–472.

Saxton, J. M. 1994. Anomalous diffusion due to obstacles: a Monte Carlo study. *Biophys. J.* 66:394–401.

Schlumpberger, T. 1999. Computational modeling of calcium action in synaptic facilitation. Ph.D. Dissertation, University of California, Berkeley, California.

Tanabe, N., and H. Kijima. 1989. Both augmentation and potentiation occur independently of internal Ca^{2+} at the frog neuromuscular junction. *Neurosci. Lett.* 99:147–152.

Tang, Y.-G., and R. S. Zucker. 1997. Mitochondrial involvement in post-tetanic potentiation of synaptic transmission. *Neuron.* 18:483–491.

Tank, D. W., W. G. Regehr, and K. R. Delaney. 1995. A quantitative analysis of presynaptic calcium dynamics that contribute to short-term enhancement. *J. Neurosci.* 15:7940–7952.

Vyshedskiy, A., and J.-W. Lin. 1997a. A study of inhibitor of the crayfish neuromuscular junction by presynaptic voltage control. *J. Neurophysiol.* 77:106–115.

Vyshedskiy, A., and J.-W. Lin. 1997b. Activation and detection of facilitation as studied by presynaptic voltage control at the inhibitor of the crayfish opener muscle. *J. Neurophysiol.* 77:2300–2315.

Wagner, J., and J. Keizer. 1994. Effects of rapid buffers on Ca^{2+} diffusion and Ca^{2+} oscillations. *Biophys. J.* 67:447–456.

Winslow, J. L., S. N. Duffy, and M. P. Charlton. 1994. Homosynaptic facilitation of transmitter release in crayfish is not affected by mobile calcium chelators: implications for the residual ionized calcium hypothesis from electrophysiological and computational analyses. *J. Neurophysiol.* 72:1769–1793.

Wright, S. N., M. S. Brodwick, and G. D. Bittner. 1996. Calcium currents, transmitter release and facilitation of release at voltage-clamped crayfish nerve terminals. *J. Physiol.* 77:2300–2315.

Xu, T., M. Naraghi, H. Kang, and E. Neher. 1997. Kinetic studies of Ca^{2+} binding and Ca^{2+} clearance in the cytosol of adrenal chromaffin cells. *Biophys. J.* 73:532–545.

Yamada, W. M., and R. S. Zucker. 1992. Time course of transmitter release calculated from simulations of a calcium diffusion model. *Biophys. J.* 61:671–682.

Zhang, L., M. G. Marcu, K. Nau-Staudt, and J. M. Trifaro. 1996. Recombinant scinderin enhances exocytosis, an effect blocked by two scinderin-derived actin-binding peptides and PIP_2. *Neuron.* 17:287–296.

Zucker, R. S. 1974. Characteristics of crayfish neuromuscular facilitation and their calcium dependence. *J. Physiol.* 241:91–110.

Zucker, R. S. 1994. Calcium and short-term synaptic plasticity. *Neth. J. Zool.* 44:495–512.

Zucker, R. S. 1999. Calcium- and activity-dependent synaptic plasticity. *Curr. Opin. Neurobiol.* 9:305–313.